

Flat Midgap Topological Surface and Hypersurface Bands without Parameter Tuning

Keun Hyuk Ahn*

Department of Physics, New Jersey Institute of Technology, Newark, New Jersey 07102, USA

The Su-Schrieffer-Heeger model is extended to the three and higher dimensional systems. Nearly or absolutely flat midgap surface and hypersurface bands are predicted based on the topological analysis, which do not require fine tuning of parameters. By adding the on-site Coulomb interaction for the three dimensional systems, we computationally show that the large difference in the band widths between the surface and the bulk leads to the strongly correlated phenomena, specifically magnetism, confined only on the surface. Possible experimental realizations in solid state materials and metamaterials are discussed.

There has been a great interest recently in flat energy or frequency bands in solid state materials and metamaterials [1–8], such as twisted bilayer graphenes [9–13] and the Lieb photonic crystals [14–17]. Flat bands could result in strongly correlated phenomena, such as magnetism and superconductivity, or localized excitations, such as trapped light and sound, which have both scientific and technological significance. However, most of these flat bands are only approximately flat, require fine tuning of parameters, touch or cross dispersive bands, involve spin-orbit interactions, exist as one-dimensional bands, or are hard to realize in solid state materials, which limit the realization of the full potentials of the flat bands [3].

In this Letter, we propose nearly or absolutely flat, midgap surface and hypersurface bands of topological origins without fine tuning of parameters or without invoking spin-orbit interactions, which are likely to be realized in solid state materials and metamaterials. This is achieved by extending the prior works by the author and collaborators [18, 19], that is, by extending the Su-Schrieffer-Heeger (SSH) model to three and higher dimensions [20–22], applying topological analyses, and computationally demonstrating that the model could host flat topological surface bands. With the Coulomb interaction considered, we further demonstrates magnetic orderings confined only on the surfaces, as an example of surface-confined strongly correlated phenomena. Discussion is provided on how such flat surface and hypersurface bands could be realized experimentally.

Starting with a simple cubic lattice with a single-site basis and a unit lattice constant, we add uniform strains, e_x , e_y , and e_z , in the x , y , and z directions, which change the lattice constants to $1+e_x$, $1+e_y$, and $1+e_z$. Further, 3D checkerboard style staggered distortions, parameterized by d_x , d_y , and d_z , are added as shown in Fig. 1, which doubles the unit cell, marked by the purple ellipse, and results in a basis of two sites, A and B . Primitive vectors \mathbf{a}_1 , \mathbf{a}_2 , and \mathbf{a}_3 are chosen as shown in Fig. 1.

With the nearest-neighbor electron hopping parameters modulated by the variations in the intersite distances, the tight binding Hamiltonian of the system with-

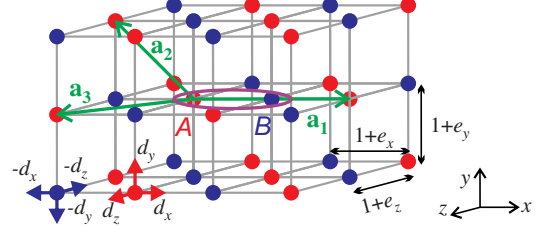


FIG. 1. 3D chiral SSH system. The purple ellipse represents the unit cell made of two sites, A and B , shown in red and blue dots. The green arrows show the primitive vectors, \mathbf{a}_1 , \mathbf{a}_2 , and \mathbf{a}_3 , and the red and blue arrows the staggered distortions parameterized by d_x , d_y , and d_z in the x , y , and z directions. $1+e_x$, $1+e_y$, and $1+e_z$ represent the intersite distances before the staggered distortions are introduced.

out surfaces is given by

$$\begin{aligned} \hat{H}_0 = & \sum_{\mathbf{R}, \sigma=\uparrow, \downarrow} -(\alpha_x + \beta_x) c_{\mathbf{R}B\sigma}^\dagger c_{\mathbf{R}A\sigma} \\ & -(\alpha_x - \beta_x) c_{\mathbf{R}+\mathbf{a}_2, B\sigma}^\dagger c_{\mathbf{R}A\sigma} - (\alpha_y + \beta_y) c_{\mathbf{R}+\mathbf{a}_3, B\sigma}^\dagger c_{\mathbf{R}A\sigma} \\ & -(\alpha_y - \beta_y) c_{\mathbf{R}B\sigma}^\dagger c_{\mathbf{R}+\mathbf{a}_1, A\sigma} - (\alpha_z + \beta_z) c_{\mathbf{R}B\sigma}^\dagger c_{\mathbf{R}+\mathbf{a}_1+\mathbf{a}_2, A\sigma} \\ & -(\alpha_y - \beta_y) c_{\mathbf{R}B\sigma}^\dagger c_{\mathbf{R}+\mathbf{a}_1+\mathbf{a}_3, A\sigma} + \text{H.c.}, \end{aligned} \quad (1)$$

where \mathbf{R} represents the Bravais lattice points, $c_{\mathbf{R}, A/B, \sigma}^\dagger$ is the creation operator for the electron with spin $\sigma = \uparrow, \downarrow$ at the A or B site within the unit cell at \mathbf{R} , and the electron hopping amplitudes are parameterized by $\alpha_a = t_0(1 - e_a)$ and $\beta_a = 2t_0d_a$ with $a=x, y, z$, and t_0 representing the nearest-neighbor hopping amplitude for the cubic lattice before the distortions. The Hamiltonian has the chiral symmetry [23], as there is no hopping between the A and A or B and B sites, which gives rise to energy levels symmetric about the zero energy. With $c_{\mathbf{R}, A/B, \sigma}^\dagger = \frac{1}{\sqrt{N_{\text{lattice}}}} \sum_{\mathbf{k}} c_{\mathbf{k}, A/B, \sigma}^\dagger e^{-i\mathbf{k} \cdot \mathbf{R}}$, $\mathbf{k} = (k_1/2\pi)\mathbf{b}_1 + (k_2/2\pi)\mathbf{b}_2 + (k_3/2\pi)\mathbf{b}_3$, \mathbf{b}_n ($n = 1, 2, 3$) representing primitive reciprocal vectors, and N_{lattice} the number of the Bravais lattice points, the Hamiltonian is represented in the form of

$$\hat{H}_0 = \sum_{\mathbf{k}, \sigma=\uparrow, \downarrow} \left[h^*(\mathbf{k}) c_{\mathbf{k}A\sigma}^\dagger c_{\mathbf{k}B\sigma} + h(\mathbf{k}) c_{\mathbf{k}B\sigma}^\dagger c_{\mathbf{k}A\sigma} \right], \quad (2)$$

SSH chains	$\alpha_x, \alpha_y, \alpha_z$	$\beta_x \beta_y \beta_z$	$\nu_1 \nu_2 \nu_3$	TI/nonTI
Along \hat{x}	$\alpha_y + \alpha_z < \alpha_x$	$\begin{smallmatrix} + & 0 & 0 \\ - & 0 & 0 \end{smallmatrix}$	$\begin{smallmatrix} 0 & 0 & 0 \\ 1 & 0 & 0 \end{smallmatrix}$	$\begin{smallmatrix} \text{nonTI} \\ \text{TI} \end{smallmatrix}$
Along \hat{y}	$\alpha_z + \alpha_x < \alpha_y$	$\begin{smallmatrix} 0 & + & 0 \\ 0 & - & 0 \end{smallmatrix}$	$\begin{smallmatrix} 0 & -1 & 0 \\ 1 & 1 & 0 \end{smallmatrix}$	$\begin{smallmatrix} \text{TI} \\ \text{TI} \end{smallmatrix}$
Along \hat{z}	$\alpha_x + \alpha_y < \alpha_z$	$\begin{smallmatrix} 0 & 0 & + \\ 0 & 0 & - \end{smallmatrix}$	$\begin{smallmatrix} 0 & 0 & -1 \\ 1 & 0 & 1 \end{smallmatrix}$	$\begin{smallmatrix} \text{TI} \\ \text{TI} \end{smallmatrix}$

TABLE I. Winding numbers ν_n ($n=1, 2, 3$) for surfaces parallel to the primitive vectors \mathbf{a}_m and $\mathbf{a}_{m'}(m, m' \neq n)$ for the 3D SSH system shown in Fig. 1. The parameters α_a and β_a ($a=x, y, z$) are the parameters in the Hamiltonian in Eq. (1), associated with the distortions. TI means topological insulator.

which leads to the spin-degenerate energy bands of $\varepsilon_{0,\pm}(\mathbf{k}) = \pm|h(\mathbf{k})|$ (see Supplemental Materials [24]).

The topological analysis is carried out in terms of three winding numbers, defined by

$$\nu_n = \frac{1}{2\pi i} \int_0^{2\pi} dk_n \frac{\partial}{\partial k_n} \ln h(k_1, k_2, k_3), \quad (3)$$

with $n = 1, 2, 3$ [18, 23, 25, 26]. The results are shown in Table I for chosen conditions, in which the systems with any nonzero winding numbers are topological insulators (TI) and would host flat midgap bands on the open surfaces perpendicular to the primitive reciprocal vectors associated with the nonzero winding numbers. We first focus on the top two rows in Table I, in which the condition of $\beta_x \neq 0$ and $\beta_y = \beta_z = 0$ describes the SSH chains running in the x direction. The condition of $\alpha_y + \alpha_z < \alpha_x$ means that the sum of the *interchain* couplings should be weaker than the average *intrachain* coupling, which is the condition for the opening of the band gap and an insulating phase for a half filling. Depending on the sign of the staggered distortion β_x the system could be either topological or nontopological insulators. A similar interpretation applies to all other cases in Table I, which represent the weakly coupled SSH chains running in y or z direction. There are two types of topological surfaces. One type occurs for the systems with $\nu_1 \neq 0$, in which the topological surfaces are perpendicular to \mathbf{b}_1 , the body-diagonal, or parallel to the plane defined by \mathbf{a}_2 and \mathbf{a}_3 , and have either A sites only or B sites only on each open surface and in each layer parallel to it. The other type occurs for the systems with $\nu_2 \neq 0$ or $\nu_3 \neq 0$, in which the topological surfaces are perpendicular to the SSH chains. In this Letter, we focus on the first type to limit the scope.

In electronic band structures, the band width reflects the energy scale for the kinetic energy. Therefore, if the band width is narrow, the effects of the Coulomb interaction would be enhanced. In the 3D topological SSH systems here, the surface band width is much narrower than the bulk band width, which means that the same Coulomb interaction would have strikingly different effects between the surface and the bulk, and could

give rise to strongly correlated phenomena only on the surfaces. To study such effects, the on-site electron-electron Coulomb interaction of U is added to the Hamiltonian in Eq. (1), which leads to the Hubbard-SSH Hamiltonian $\hat{H} = \hat{H}_0 + \hat{H}_C$ with $\hat{H}_C = \sum_{\mathbf{R}} U \hat{\rho}_{\mathbf{R}A\uparrow} \hat{\rho}_{\mathbf{R}A\downarrow} + U \hat{\rho}_{\mathbf{R}B\uparrow} \hat{\rho}_{\mathbf{R}B\downarrow}$, representing the on-site Coulomb interaction, and $\hat{\rho}_{\mathbf{R},A/B,\sigma} = c_{\mathbf{R},A/B,\sigma}^\dagger c_{\mathbf{R},A/B,\sigma}$ the number operator. Within the Hartree-Fock approximation, the Hamiltonian is transformed to \hat{H}_{HF} shown below, which is solved recursively till the self-consistency is reached.

$$\hat{H}_{\text{HF}} = \hat{H}_0 + \hat{H}_{C,\text{HF}} \quad (4)$$

$$\hat{H}_{C,\text{HF}} = \sum_{\mathbf{R}} U \hat{\rho}_{\mathbf{R}A\uparrow} \langle \hat{\rho}_{\mathbf{R}A\downarrow} \rangle + U \langle \hat{\rho}_{\mathbf{R}A\uparrow} \rangle \hat{\rho}_{\mathbf{R}A\downarrow} + U \hat{\rho}_{\mathbf{R}B\uparrow} \langle \hat{\rho}_{\mathbf{R}B\downarrow} \rangle + U \langle \hat{\rho}_{\mathbf{R}B\uparrow} \rangle \hat{\rho}_{\mathbf{R}B\downarrow} \quad (5)$$

Various periodicities are considered and the lowest energy states are found for the cases with $\beta_x \neq 0$ in Table I. We first study the systems without any surfaces. To be specific, the parameter values are chosen as shown in the caption of Fig. 2, and we seek trends in numerical results. For the $U=0$ case, the ground state is nonmagnetic and, for the chosen parameter values, the width of each band is about 2.7 and the size of the gap about 0.7. As the Coulomb interaction U increases past $U_c \approx 2.0$, the same order of magnitude as the band width, the ground state changes to a 3D checkerboard-type antiferromagnetic state with A and B sites having the opposite spin directions.

Numerical approaches are used to study the systems with the open surfaces parallel to \mathbf{a}_2 and \mathbf{a}_3 . The total number of layers is $L_1 = 2N_1$ if both surfaces are made of full unit cells, and $L_1 = 2N_1 + 1$ if one surface is made of half unit cells, where N_1 represents the number of full unit cells along the \mathbf{a}_1 direction. Figure 2 shows the band structures for the systems with open surfaces, before the Coulomb term, $\hat{H}_{C,\text{HF}}$, is included. The band structures for the nonTI and TI systems are shown in Figs. 2(a) and 2(b), respectively, with $N_1 = 4$ and full unit cells on both surfaces, which reveal clear differences. While the nonTI band structure in Fig. 2(a) has no bands in the gap, the TI band structure in Fig. 2(b) has two surface bands in the gap, marked by the green triangles, consistent with the topological analysis. The small dispersions (about 0.28) for each surface band and the tiny separation (about 0.04) between them in Fig. 2(b) are the results of the hybridization of the surface bands from the opposite surfaces, similar to the 1D and 2D SSH systems [18, 19, 23]. One way to reduce the hybridization is to increase the separation between the open surfaces, as demonstrated by the band structures for a thicker, $N_1 = 12$, TI system in Fig. 2(c). The two midgap surface bands are indeed almost completely flat (the width of about 0.03) and their separation is greatly reduced (down to 4×10^{-5}). Another way to achieve flatter, in fact *absolutely* flat, surface bands is to eliminate the surface band

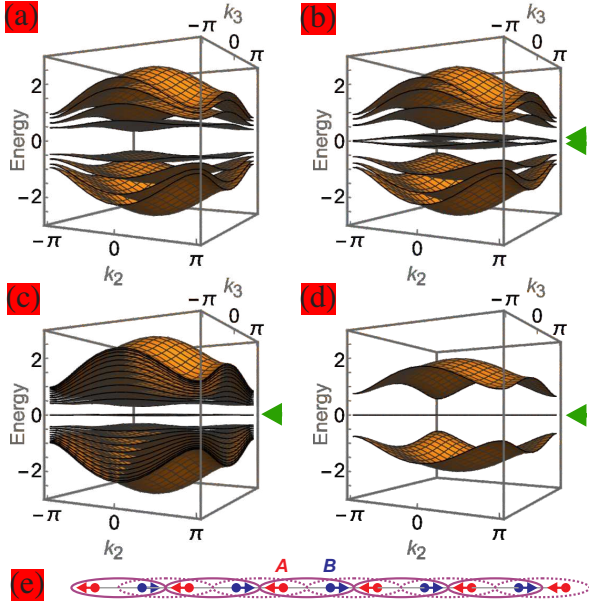


FIG. 2. (a-d): Band structures for the 3D SSH systems with open surfaces before the Hubbard term is considered. (e): 1D SSH chain with a half unit cell on one edge. (a-c) show the results for systems with full unit cells on both surfaces, while (d) for a system with half unit cells on one surface. The green triangles mark the surface bands. Common parameter values are $\alpha_x=1.0$, $\alpha_y=0.3$, $\alpha_z=0.2$, $\beta_y=\beta_z=0$, while varied parameter values of N_1 and β_x are 4 and 0.2 for (a), 4 and -0.2 for (b), 12 and -0.2 for (c), and 1 and ± 0.2 for (d). In the 1D SSH system in (e), the unit cells chosen from the left and right edges, marked by ellipses in solid and dotted lines, respectively, indicate that one edge (the left edge for the shown distortions) is topological and the other nontopological [27, 28].

on the other surface by making it locally equivalent to the nontopological surface. This is achieved by having half unit cells on one surface. In this case, analogous to the 1D SSH system shown in Fig. 2(e) [27, 28], the unique characteristics of the SSH chain make one surface topological and the other nontopological regardless of the sign of the staggered distortion β_x , and the topological midgap surface band is present only on one surface and absolutely flat. The band structure in Fig. 2(d) for $N_1=1$ with $\beta_x \neq 0$ shows that, unlike the full unit cell TI in Fig. 2(b), only one spin-degenerate surface band exists and is completely flat with energy zero [24]. The 3D SSH systems here, regardless of full or half unit cells on the surfaces, have the chiral symmetry, which guarantees that the eigenstates appear in pairs with the energies $\pm \varepsilon(\mathbf{k}_{\parallel})$ at each wavevector \mathbf{k}_{\parallel} parallel to the surface [23]. If the number of layers is odd, the chiral symmetry forces at least one eigenstate to have a zero energy at each \mathbf{k}_{\parallel} , and the system has at least one completely flat band, as Fig. 2(d) shows.

The striking band width difference between the surface and the bulk seen here for the TI systems provides the opportunity to create strongly correlated phases only

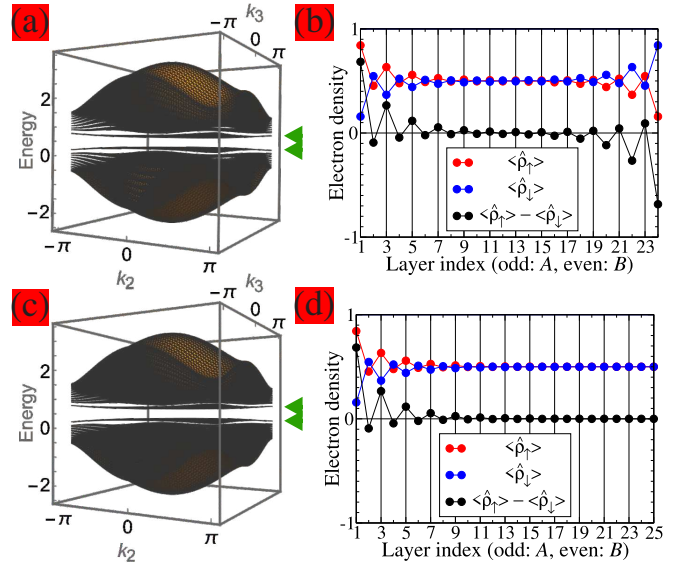


FIG. 3. Results for the 3D Hubbard SSH systems with open surfaces within the Hartree-Fock approximations. (a), (b): for the system with full unit cells on both surfaces. (c), (d): for the system with half unit cells on one surface. (a), (c): the band structures with green triangles marking the surface bands. (b), (d): the profiles for the spin up and spin down electron densities and their difference, that is, $\langle \hat{\rho}_{\uparrow} \rangle$, $\langle \hat{\rho}_{\downarrow} \rangle$, and $\langle \hat{\rho}_{\uparrow} \rangle - \langle \hat{\rho}_{\downarrow} \rangle$, versus the index of layers. The Coulomb interaction is $U=1.0$, and other parameter values are identical to those for Fig. 2(c).

on the surfaces, not in the bulk. We choose the on-site Coulomb interaction $U=1.0$, greater than the surface band width but less than the bulk band width, and find the ground state. The results are shown in Fig. 3. Figure 3(a) shows the spin degenerate band structure for the TI systems with full unit cells on both surfaces and $N_1=12$. Comparison with Fig. 2(c) reveals that the two surface bands, marked by the green triangles in Fig. 3(a), split by about U , while each surface band remaining quite narrow. The spin up and spin down electron densities, represented by $\langle \hat{\rho}_{\uparrow} \rangle$ and $\langle \hat{\rho}_{\downarrow} \rangle$, are found to be constant in the \mathbf{a}_2 and \mathbf{a}_3 directions, but modulating along the \mathbf{a}_1 direction while maintaining the total electron density constant, that is, $\langle \hat{\rho}_{\uparrow} \rangle + \langle \hat{\rho}_{\downarrow} \rangle = 1$. Figure 3(b) shows the profiles of the spin up and spin down electron densities and their difference along the \mathbf{a}_1 direction in red, blue, and black symbols, respectively. The results show that the net magnetic moment (black symbols) has the greatest magnitude at the open surfaces, and decays rapidly towards the interior with the sign alternating between the A and B layers, demonstrating different effects of the Coulomb interaction on the surfaces and the bulk.

The electron density profiles for the system with half unit cells on one surface for the same $U=1.0$, shown in Fig. 3(d), is quite different. The net magnetic moment (black symbols) appears only on one surface, but

is absent on the other, as only one surface hosts the flat topological surface band. Although its band structure in Fig. 3(c) may look overall similar to that in Fig. 3(a), the two flat surface bands, marked by green triangles, have opposite spins and all the surface and bulk bands are nondegenerate, as the electron density profile in Fig. 3(d) breaks the global spin symmetry.

The large difference between the surface and the bulk band widths seen in Fig. 2 manifests itself as very different critical Coulomb interactions for the magnetizations of the surface and the bulk. The spin polarization, defined as $|\langle\hat{\rho}_\uparrow\rangle - \langle\hat{\rho}_\downarrow\rangle|$, versus the Coulomb interaction U for the systems with full unit cells on both surfaces is displayed in Fig. 4(a). The result for the system without surfaces is also shown in green solid line. For the thin system with $N_1=4$ (blue symbols), the surface spin polarization (blue circles) starts to appear at around $U_{c,s}\approx 0.42$, the same order of magnitude as the width of each surface band (about 0.28) in Fig. 2(b), and increases rapidly, approaching to the full spin polarization of 1.0. As for the bulk spin polarization (blue squares), defined as $|\langle\hat{\rho}_\uparrow\rangle - \langle\hat{\rho}_\downarrow\rangle|$ at the center layer, although it appears at the same $U\approx U_{c,s}\approx 0.42$ as the surface spin polarization and increases slowly, this is the tail of the surface spin polarization seen in Fig. 3(b), and the *intrinsic* bulk spin polarization develops rapidly only above $U_{c,b}\approx 2.0$, same as U_c for the system without surfaces (see the green line). As the system becomes thicker to $N_1=12$ (red symbols), the surface band becomes much narrower, as seen in Fig. 2(c), and the surface spin polarization (red circles) appears from around $U_{c,s}\approx 0.0025$ as revealed in the inset, about 200 times smaller than that of $N_1=4$ system. The tails of the surface states are suppressed substantially at the center layer and the bulk spin polarization (red squares) remains negligible until the intrinsic bulk spin polarization develops at around $U_{c,b}\approx 2.0$. Further studies on the systems with $N_1=6, 8, 10$ reveal that the decay in $U_{c,s}$ with respect to N_1 is exponential, reflecting the exponentially decaying surface band width [19] (see Supplemental Materials for the phase diagrams [24]).

The spin polarization versus the Coulomb interaction for the systems with one surface made of half unit cells is shown in Fig. 4(b). Because the surface band for $U=0$ is absolutely flat, as seen in Fig. 2(d), any nonzero Coulomb interaction U gives rise to the magnetization on the topological surface, as shown in Fig. 4(b) and its inset for $N_1=4$ (blue circles) and $N_1=12$ (red circles). For the thin $N_1=4$ systems, the tails of the surface states show up as finite spin polarizations in the center layer of the bulk (blue squares) and even on the nontopological surface (blue triangles). Similar to Fig. 4(a), such spin polarizations decrease rapidly when the system thickness increases to $N_1=12$ (red squares and red triangles).

By making artificial connections, metamaterials with effective dimensions higher than three could be created [20–22]. Therefore, the extension of the 3D SSH

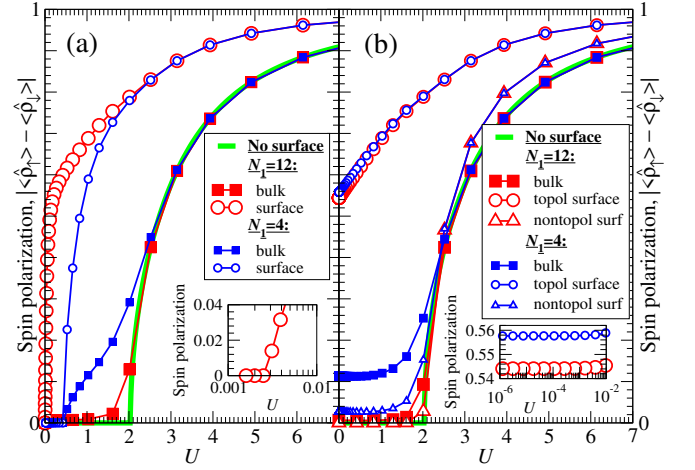


FIG. 4. Surface and bulk spin polarizations, $|\langle\hat{\rho}_\uparrow\rangle - \langle\hat{\rho}_\downarrow\rangle|$, versus the Coulomb interaction U for the 3D Hubbard SSH systems. (a) for the systems with full unit cells on both surfaces, and (b) for the systems with half unit cells on one surface. The thick systems with $N_1=12$ (red symbols) and the thin systems with $N_1=4$ (blue symbols) are considered. Other parameter values are identical to those in Figs. 2(c) and 3. The green lines show the results for the systems without open surfaces. The circles and squares represent the spin polarization on the topological surfaces and at the center layer in the bulk, respectively. The triangles in (b) represent the spin polarization on nontopological surfaces. The insets show the spin polarization at small U 's in semilogarithmic scales.

model to higher ND is of interest. As in the 3D SSH models, the ND chiral SSH model is made of 1D SSH chains coupled in the $N-1$ dimensional directions, with neighboring chains shifted with respect to each other and the A sites surrounded by the B sites and vice versa. These 1D SSH chains should couple weakly to open a band gap. Specifically, the sum of the *interchain* couplings should be weaker than the average *intrachain* coupling. With the primitive vectors of the ND SSH system defined in the way analogous to those in Fig. 1, the N winding numbers are defined. Just like the 3D SSH systems, there could be two kinds of topological hypersurfaces. The first is perpendicular to the ND diagonal direction, and the second perpendicular to the SSH chains. Further details, including ND SSH Hamiltonian, energy bands, winding numbers, topological analysis, and nearly or absolutely flat, topological, midgap hypersurface bands, are given in Supplemental Materials [24].

For the 3D SSH systems, it would be fruitful for the future studies to investigate the possibility of other strongly correlated phenomena, particularly, unconventional superconductivity [29, 30], similar to that in twisted bilayer graphenes [10, 11]. Realizing 3D SSH systems experimentally would require either building artificial structures [31], such as 3D quantum dot arrays [28, 32–36], or solid state materials search using first-principles calculations and topological indices, as done by Jeon and

Kim [8]. The higher ND SSH systems would be realized by building multiple 3D systems and connecting them using electronics that mimic the higher dimensional interactions [20–22].

In summary, we have proposed the chiral extension of the SSH model to three dimensions, and showed that it could give rise to topological insulators with flat midgap surface bands. It is demonstrated that the Coulomb interaction could result in magnetism confined only on the topological surfaces. The extension to higher dimensions is presented.

* kenahn@njit.edu

- [1] J. T. Chalker, T. S. Pickles, and P. Shukla, Anderson localization in tight-binding models with flat bands, *Phys. Rev. B* **82**, 104209 (2010).
- [2] E. J. Bergholtz and Z. Liu, Topological flat band models and fractional Chern insulators, *Int. J. Mod. Phys. B* **27**, 1330017 (2013).
- [3] D. Leykam, A. Andreanov, and S. Flach, Artificial flat band systems: From lattice models to experiments, *Adv. Phys. X* **3**, 1473052 (2018).
- [4] J.-W. Rhim and B.-J. Yang, Singular flat bands, *Adv. Phys. X* **6**, 1 (2021).
- [5] J. G. Checkelsky, B. A. Bernevig, P. Coleman, Q. Si and S. Paschen, Flat bands, strange metals and the Kondo effect, *Nat. Rev. Mater.* **9**, 509 (2024).
- [6] W.-X. Qiu, S. Li, J.-H. Gao, Y. Zhou, and F.-C. Zhang, Designing an artificial Lieb lattice on a metal surface, *Phys. Rev. B* **94**, 241409(R) (2016).
- [7] M. R. Slot, T. S. Gardenier, P. H. Jacobse, G. C. P. van Miert, S. N. Kempkes, S. J. M. Zevenhuizen, C. M. Smith, D. Vanmaekelbergh, and I. Swart, Experimental realization and characterization of an electronic Lieb lattice, *Nature Phys.* **13**, 672 (2017).
- [8] S. Jeon and Y. Kim, Two-dimensional weak topological insulators in inversion-symmetric crystals, *Phys. Rev. B* **105**, L121101 (2022).
- [9] R. Bistritzer and A. H. MacDonald, Moiré bands in twisted double-layer graphene, *Proc. Nat. Acad. Sci.* **108**, 12233 (2011).
- [10] Y. Cao, V. Fatemi, S. Fang, K. Watanabe, T. Taniguchi, E. Kaxiras, and P. Jarillo-Herrero, Unconventional superconductivity in magic-angle graphene superlattices, *Nature* **556**, 43 (2018).
- [11] Y. Cao, V. Fatemi, A. Demir, S. Fang, S. L. Tomarken, J. Y. Luo, J. D. Sanchez-Yamagishi, K. Watanabe, T. Taniguchi, E. Kaxiras, R. C. Ashoori, and P. Jarillo-Herrero, Correlated insulator behaviour at half-filling in magic-angle graphene superlattices, *Nature* **556**, 80 (2018).
- [12] E. Y. Andrei and A. H. MacDonald, Graphene bilayers with a twist. *Nat. Mater.* **19**, 1265 (2020).
- [13] P. Törmä, S. Peotta, and B. A. Bernevig, Superconductivity, superfluidity and quantum geometry in twisted multilayer systems, *Nat. Rev. Phys.* **4**, 528 (2022).
- [14] E. H. Lieb, Two Theorems on the Hubbard Model, *Phys. Rev. Lett.* **62**, 1201 (1989).
- [15] S. Mukherjee, A. Spracklen, D. Choudhury, N. Goldman, P. Öhberg, E. Andersson, and R. R. Thomson, Observation of Localized States in Lieb Photonic Lattices, *Phys. Rev. Lett.* **114**, 245504 (2015).
- [16] R. A. Vicencio, C. Cantillano, L. Morales-Inostroza, B. Real, C. Mejía-Cortés, S. Weimann, A. Szameit, and M. I. Molina, Observation of a Localized Flat-Band State in a Photonic Lieb Lattice, *Phys. Rev. Lett.* **114**, 245503 (2015).
- [17] D. S. Wiersma, Trapped in a Photonic Maze, *Physics* **8**, 55 (2015).
- [18] L. Zhu, E. Prodan, and K. H. Ahn, Flat energy bands within antiphase and twin boundaries and at open edges in topological materials, *Phys. Rev. B* **99**, 041117(R) (2019).
- [19] K. Qian, L. Zhu, K. H. Ahn, and C. Prodan, Observation of flat frequency bands at open edges and antiphase boundary seams in topological mechanical metamaterials, *Phys. Rev. Lett.* **125**, 225501 (2020).
- [20] T. Ozawa, H. M. Price, Topological quantum matter in synthetic dimensions, *Nat. Rev. Phys.* **1**, 349 (2019).
- [21] H. Price, Simulating four-dimensional physics in the laboratory, *Physics Today* **75** (4), 38 (2022).
- [22] Y. Wang, H. M. Price B. Zhang, and Y. D. Chong, Circuit implementation of a four-dimensional topological insulator, *Nat. Commun.* **11**, 2356 (2020).
- [23] J. K. Asbóth, L. Oroszlány, and A. Pályi, *A Short Course on Topological Insulators: Band Structure and Edge States in one and Two Dimensions* (Springer, Cham, 2016).
- [24] See Supplemental Materials at <http://...> for the 3D Hamiltonian and energy bands for the systems without surfaces, the 3D Hamiltonians for the systems with surfaces, the phase diagrams in the plane of the Coulomb interaction versus the system thickness, and ND SSH Hamiltonian and its topological analysis.
- [25] P. Delplace, D. Ullmo, and G. Montambaux, Zak phase and the existence of edge states in graphene *Phys. Rev. B* **84**, 195452 (2011).
- [26] J. Zak, Berry's phase for energy bands in solids, *Phys. Rev. Lett.* **62**, 2747 (1989).
- [27] C. Prodan (private communication)
- [28] M. Benito, M. Niklas, G. Platero, and S. Kohler, Edge-state blockade of transport in quantum dot arrays, *Phys. Rev. Lett.* **90**, 067204 (2016).
- [29] V. I. Iglovikov, F. Hébert, B. Grémaud, G. G. Batrouni, and R. T. Scalettar, Superconducting transitions in flat-band systems, *Phys. Rev. B* **90**, 094506 (2014).
- [30] V. Peri, Z.-D. Song, B. A. Bernevig, and S. D. Huber, Fragile Topology and Flat-Band Superconductivity in the Strong-Coupling Regime, *Phys. Rev. Lett.* **126**, 027002 (2021).
- [31] I. Belopolski, S.-Y. Xu, N. Koirala, C. Liu, G. Bian, V. N. Strocov, G. Chang, M. Neupane, N. Alidoust, D. Sanchez, H. Zheng, M. Brahlek, V. Rogalev, T. Kim, N. C. Plumb, C. Chen, F. Bertran, P. Le Fèvre, A. Taleb-Ibrahimi, M.-C. Asensio, M. Shi, H. Lin, M. Hoesch, S. Oh, M. Z. Hasan, A novel artificial condensed matter lattice and a new platform for one-dimensional topological phases, *Sci. Adv.* **3**, e1501692 (2017).
- [32] S. M. Reimann and M. Manninen, Electronic structure of quantum dots, *Rev. Mod. Phys.* **74** 1283 (2002).
- [33] H. Tamura, K. Shiraishi, T. Kimura, and H. Takayanagi, Flat-band ferromagnetism in quantum dot superlattices, *Phys. Rev. B* **65**, 085324 (2002).

- [34] H. Tamura, K. Shiraishi, and H. Takayanagi, *Quantum dot atoms, molecules, and superlattices*, in *Quantum Dots and Nanowires*, edited by S. Bandyopadhyay and H. S. Nalwa (American Scientific Publisher, USA, 2003), Chapter 2.
- [35] I. Piquero-Zulaica, J. Lobo-Checa, A. Sadeghi, Z. M. A. El-Fattah, C. Mitsui, T. Okamoto, R. Pawlak, T. Meier, A. Arnau, J. E. Ortega, J. Takeya, S. Goedecker, E. Meyer, and S. Kawai, Precise engineering of quantum dot array coupling through their barrier widths, *Nat. Commun.* **8**, 787 (2017).
- [36] D. M. T. Kuo, High thermoelectric figure of merit of quantum dot array quantum wires, *Jpn. J. Appl. Phys.* **60**, 075001 (2021).

Supplemental Material for "Flat Midgap Topological Surface and Hypersurface Bands without Parameter Tuning"

Keun Hyuk Ahn

Department of Physics, New Jersey Institute of Technology, Newark, New Jersey 07102, USA

I. HAMILTONIANS AND ENERGY BANDS FOR THREE-DIMENSIONAL SU-SCHRIEFFER-HEEGER SYSTEMS

The off-diagonal element $h(\mathbf{k})$ in Eq. (2) in the main text is as follows.

$$h(\mathbf{k}) = -(\alpha_x + \beta_x) - (\alpha_x - \beta_x)e^{ik_1} - (\alpha_y + \beta_y)e^{-ik_2} - (\alpha_y - \beta_y)e^{i(k_1+k_2)} - (\alpha_z + \beta_z)e^{-ik_3} - (\alpha_z - \beta_z)e^{i(k_1+k_3)} \quad (S1)$$

The bulk energy bands in the absence of the Coulomb interaction is given by

$$\varepsilon_{\pm}(\mathbf{k}) = \pm 2 \left\{ \left[\alpha_x \cos \frac{k_1}{2} + \alpha_y \cos \left(\frac{k_1}{2} + k_2 \right) + \alpha_z \cos \left(\frac{k_1}{2} + k_3 \right) \right]^2 + \left[\beta_x \sin \frac{k_1}{2} + \beta_y \sin \left(\frac{k_1}{2} + k_2 \right) + \beta_z \sin \left(\frac{k_1}{2} + k_3 \right) \right]^2 \right\}^{1/2}. \quad (S2)$$

The surface breaks the translational symmetry in one direction, but maintains it in other directions. The three-dimensional (3D) Su-Schrieffer-Heeger (SSH) systems with the surfaces parallel to \mathbf{a}_2 and \mathbf{a}_3 , the thickness $L_1 = 2N_1$, and the full unit cells on both surfaces are represented by the following Hamiltonian in the absence of the Coulomb interaction:

$$\hat{H}_0 = \sum_{\mathbf{k}_{\parallel}, \sigma=\uparrow, \downarrow} \begin{pmatrix} C_{\mathbf{k}_{\parallel} A\sigma}^{\dagger} \\ C_{\mathbf{k}_{\parallel} B\sigma}^{\dagger} \end{pmatrix}^T \begin{pmatrix} 0 & h_{N_1 \times N_1}^{\dagger}(\mathbf{k}_{\parallel}) \\ h_{N_1 \times N_1}(\mathbf{k}_{\parallel}) & 0 \end{pmatrix} \begin{pmatrix} C_{\mathbf{k}_{\parallel} A\sigma} \\ C_{\mathbf{k}_{\parallel} B\sigma} \end{pmatrix}, \quad (S3)$$

where $\mathbf{k}_{\parallel} = (k_2/2\pi)\mathbf{b}_2 + (k_3/2\pi)\mathbf{b}_3$, $C_{\mathbf{k}_{\parallel}, A/B, \sigma}^{\dagger} = (c_{1, \mathbf{k}_{\parallel}, A/B, \sigma}^{\dagger}, c_{2, \mathbf{k}_{\parallel}, A/B, \sigma}^{\dagger}, \dots, c_{N_1, \mathbf{k}_{\parallel}, A/B, \sigma}^{\dagger})$, and the $N_1 \times N_1$ matrix $h_{N_1 \times N_1}(\mathbf{k}_{\parallel})$ is

$$h_{N_1 \times N_1}(\mathbf{k}_{\parallel}) = \begin{pmatrix} \gamma_0 & \gamma_1 & 0 & \dots & 0 & 0 & 0 \\ 0 & \gamma_0 & \gamma_1 & \dots & 0 & 0 & 0 \\ 0 & 0 & \gamma_0 & \dots & 0 & 0 & 0 \\ \vdots & \vdots & \vdots & \ddots & \vdots & \vdots & \vdots \\ 0 & 0 & 0 & \dots & \gamma_0 & \gamma_1 & 0 \\ 0 & 0 & 0 & \dots & 0 & \gamma_0 & \gamma_1 \\ 0 & 0 & 0 & \dots & 0 & 0 & \gamma_0 \end{pmatrix} \quad (S4)$$

with $\gamma_0(\mathbf{k}_{\parallel}) = -[(\alpha_x + \beta_x) + (\alpha_y + \beta_y)e^{-ik_2} + (\alpha_z + \beta_z)e^{-ik_3}]$ and $\gamma_1(\mathbf{k}_{\parallel}) = -[(\alpha_x - \beta_x) + (\alpha_y - \beta_y)e^{ik_2} + (\alpha_z - \beta_z)e^{ik_3}]$.

As discussed in the main text, we also consider the 3D SSH systems with the open surfaces parallel to \mathbf{a}_2 and \mathbf{a}_3 and the half unit cells on one surface, which have the thickness $L_1 = 2N_1 + 1$ and $N_1 + 1$ of A sites and N_1 of B sites in \mathbf{a}_1 direction. Such systems are described by the Hamiltonian given by

$$\hat{H}_0 = \sum_{\mathbf{k}_{\parallel}, \sigma=\uparrow, \downarrow} \begin{pmatrix} C_{\mathbf{k}_{\parallel} A\sigma}^{\dagger} \\ C_{\mathbf{k}_{\parallel} B\sigma}^{\dagger} \end{pmatrix}^T \begin{pmatrix} 0 & h_{(N_1+1) \times N_1}^{\dagger}(\mathbf{k}_{\parallel}) \\ h_{N_1 \times (N_1+1)}(\mathbf{k}_{\parallel}) & 0 \end{pmatrix} \begin{pmatrix} C_{\mathbf{k}_{\parallel} A\sigma} \\ C_{\mathbf{k}_{\parallel} B\sigma} \end{pmatrix}, \quad (S5)$$

where $C_{\mathbf{k}_{\parallel} A\sigma}^{\dagger} = (c_{1, \mathbf{k}_{\parallel}, A\sigma}^{\dagger}, c_{2, \mathbf{k}_{\parallel}, A\sigma}^{\dagger}, \dots, c_{N_1, \mathbf{k}_{\parallel}, A\sigma}^{\dagger}, c_{N_1+1, \mathbf{k}_{\parallel}, A\sigma}^{\dagger})$, $C_{\mathbf{k}_{\parallel} B\sigma}^{\dagger} = (c_{1, \mathbf{k}_{\parallel}, B\sigma}^{\dagger}, c_{2, \mathbf{k}_{\parallel}, B\sigma}^{\dagger}, \dots, c_{N_1, \mathbf{k}_{\parallel}, B\sigma}^{\dagger})$, and the $N_1 \times (N_1 + 1)$ matrix $h_{N_1 \times (N_1+1)}(\mathbf{k}_{\parallel})$ is

$$h_{N_1 \times (N_1+1)}(\mathbf{k}_{\parallel}) = \begin{pmatrix} \gamma_0 & \gamma_1 & 0 & \dots & 0 & 0 & 0 & 0 \\ 0 & \gamma_0 & \gamma_1 & \dots & 0 & 0 & 0 & 0 \\ 0 & 0 & \gamma_0 & \dots & 0 & 0 & 0 & 0 \\ \vdots & \vdots & \vdots & \ddots & \vdots & \vdots & \vdots & \vdots \\ 0 & 0 & 0 & \dots & \gamma_0 & \gamma_1 & 0 & 0 \\ 0 & 0 & 0 & \dots & 0 & \gamma_0 & \gamma_1 & 0 \\ 0 & 0 & 0 & \dots & 0 & 0 & \gamma_0 & \gamma_1 \end{pmatrix} \quad (S6)$$

with $\gamma_0(\mathbf{k}_{\parallel})$ and $\gamma_1(\mathbf{k}_{\parallel})$ identical to those in Eq. (S4). The special case of $N_1=1$ and $\beta_y=\beta_z=0$ results in two bulk bands and one absolutely flat midgap band given by

$$\varepsilon_0(\mathbf{k}_{\parallel}) = 0, \quad (S7)$$

$$\varepsilon_{\pm}(\mathbf{k}_{\parallel}) = \pm \sqrt{2} \left[(\alpha_x + \alpha_y \cos k_2 + \alpha_z \cos k_3)^2 + \beta_x^2 + (\alpha_y \sin k_2 + \alpha_z \sin k_3)^2 \right]^{1/2}. \quad (S8)$$

The 3D Hubbard SSH Hamiltonians with the open surfaces are obtained by adding the diagonal on-site Hubbard terms to Eqs. (S3) and (S5), which are analyzed through the Hartree-Fock approximation as presented in the main text.

II. PHASE DIAGRAMS

The phase diagrams in the semilogarithmic U - N_1 plane are shown in Fig. S1(a) for the 3D topological Hubbard

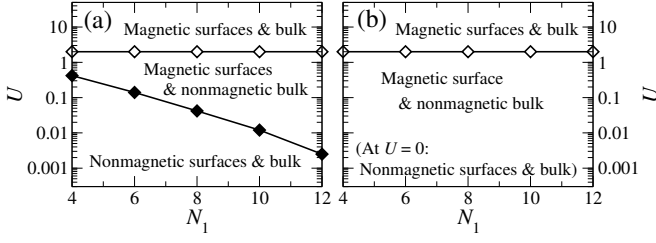


FIG. S1. Phase diagrams in semilogarithmic U - N_1 planes, (a) for the 3D topological Hubbard SSH systems with the full unit cells on both surfaces, and (b) for those with the half unit cells on one surface and full unit cells on the other. U represents the on-site Coulomb interaction and N_1 the number of the full unit cells in \mathbf{a}_1 direction. The parameter values are identical to those in Figs. 2(c), 3, and 4 in the main text, except U and N_1 varied here.

SSH systems with the full unit cells on both surfaces and in Fig. S1(b) for those with the half unit cells on one surface, which show the regions with the magnetic moments confined only on the topological surfaces. For the topological systems with full unit cells on both surfaces, the critical Coulomb interaction for the surface spin polarization, $U_{c,s}$, shown in solid symbols in Fig. S1(a), decays exponentially as N_1 increases, reflecting the exponentially decaying surface band widths, as found for the 2D SSH systems [S1]. In contrast, for the systems with half unit cells on one surface in Fig. S1(b), the surface spin polarization appears for any nonzero Coulomb interactions, as the surface band is absolutely flat. The critical Coulomb interaction for the intrinsic bulk spin polarization, $U_{c,b}$, shown in open symbols in Figs. S1(a) and S1(b), remains independent of the system thickness, as the bulk band width is approximately unchanged.

III. ND SSH HAMILTONIAN AND TOPOLOGICAL ANALYSIS

The SSH model is generalized to the arbitrary N -dimensional space. Analogous to the 3D SSH system in Fig. 1 in the main text, we start with a ND hypercubic lattice, and add uniform and staggered distortions parameterized by e_n and d_n , respectively, in the x_n direction, where $n=1, 2, \dots, N$. Expressed in the Cartesian unit vectors, primitive vectors are chosen as $\mathbf{a}_1 = 2(1 + e_1)\hat{\mathbf{x}}_1$, $\mathbf{a}_2 = -(1 + e_1)\hat{\mathbf{x}}_1 + (1 + e_2)\hat{\mathbf{x}}_2$, $\mathbf{a}_3 = -(1 + e_1)\hat{\mathbf{x}}_1 + (1 + e_3)\hat{\mathbf{x}}_3, \dots, \mathbf{a}_N = -(1 + e_1)\hat{\mathbf{x}}_1 + (1 + e_N)\hat{\mathbf{x}}_N$. The two-site basis is made of an A site at $\sum_{n=1}^N d_n \hat{\mathbf{x}}_n$ and a B site at $(1 + e_1)\hat{\mathbf{x}}_1 - \sum_{n=1}^N d_n \hat{\mathbf{x}}_n$.

With t_0 representing the nearest neighbor hopping amplitude for the ND hypercubic lattice before the distortions are applied, the Hamiltonian for the ND SSH sys-

tem is given by

$$\hat{H}_0 = \sum_{\mathbf{R}} \left[-(\alpha_1 + \beta_1)c_{\mathbf{R}B}^\dagger c_{\mathbf{R}A} - (\alpha_1 - \beta_1)c_{\mathbf{R}B}^\dagger c_{\mathbf{R}+\mathbf{a}_1,A} - \sum_{n=2}^N (\alpha_n + \beta_n)c_{\mathbf{R}+\mathbf{a}_n,B}^\dagger c_{\mathbf{R}A} - (\alpha_n - \beta_n)c_{\mathbf{R}B}^\dagger c_{\mathbf{R}+\mathbf{a}_1+\mathbf{a}_n,A} \right] + H.c., \quad (\text{S9})$$

where $\alpha_n = t_0(1 - e_n)$ and $\beta_n = 2t_0d_n$ represent the linear modulation of the hopping parameters by the distortions and the spin indices are omitted. Similar to the 3D SSH model, the Hamiltonian in reciprocal space is given by

$$\hat{H}_0 = \sum_{\mathbf{k}} \begin{pmatrix} c_{\mathbf{k}A}^\dagger & c_{\mathbf{k}B}^\dagger \end{pmatrix} \begin{pmatrix} 0 & h^*(\mathbf{k}) \\ h(\mathbf{k}) & 0 \end{pmatrix} \begin{pmatrix} c_{\mathbf{k}A} \\ c_{\mathbf{k}B} \end{pmatrix}, \quad (\text{S10})$$

where $\mathbf{k} = (k_1/2\pi)\mathbf{b}_1 + (k_2/2\pi)\mathbf{b}_2 + \dots + (k_N/2\pi)\mathbf{b}_N$ with \mathbf{b}_n ($n=1, 2, \dots, N$) representing the primitive reciprocal vectors and $h(\mathbf{k}) = -[(\alpha_1 + \beta_1) + (\alpha_1 - \beta_1)e^{ik_1}] - \sum_{n=2}^N [(\alpha_n + \beta_n)e^{-ik_n} + (\alpha_n - \beta_n)e^{i(k_1+k_n)}]$. The above Hamiltonian leads to the energy bands given by

$$\varepsilon_{\pm}(\mathbf{k}) = \pm 2 \left\{ \left[\alpha_1 \cos \frac{k_1}{2} + \sum_{n=2}^N \alpha_n \cos \left(\frac{k_1}{2} + k_n \right) \right]^2 + \left[\beta_1 \sin \frac{k_1}{2} + \sum_{n=2}^N \beta_n \sin \left(\frac{k_1}{2} + k_n \right) \right]^2 \right\}^{1/2}. \quad (\text{S11})$$

The gap opens and the system becomes an insulator for a half filling, if the system is made of weakly coupled SSH chains, that is, if $\beta_n \neq 0$, $\beta_{m \neq n} = 0$, and $\alpha_n > \sum_{m \neq n} \alpha_m$ for $n = 1, 2, \dots$, or N .

The topological analysis is carried out in terms of the winding numbers, $\nu_1, \nu_2, \dots, \nu_N$, defined by

$$\nu_n = \frac{1}{2\pi i} \int_0^{2\pi} dk_n \frac{\partial}{\partial k_n} \ln h(k_1, k_2, \dots, k_N), \quad (\text{S12})$$

with $n = 1, 2, \dots, N$. Table S1 shows how the winding numbers depend on the parameters, which reveals that the system is a topological insulator except when $\beta_1 > 0$, $\beta_{m \neq 1} = 0$ and $\alpha_1 > \sum_{m \neq 1} \alpha_m$. As the nonzero winding numbers dictate the directions of the topological hypersurfaces, Table S1 also illustrates that there are two types of topological hypersurfaces. One is the type of the hypersurfaces that are perpendicular to \mathbf{b}_1 , that is, parallel to $\mathbf{a}_2, \mathbf{a}_3, \dots$, and \mathbf{a}_N , for the cases with $\nu_1 = 1$. In this type, the open hypersurfaces have the A sites only or the B sites only, as in the 3D SSH systems. The other is the type of the hypersurfaces that are perpendicular to the SSH chains for the cases with $\nu_{n \neq 1} = \pm 1$. In this type, the open hypersurfaces would have the alternating A and B sites in a $(N-1)$ -dimensional checkerboard pattern. These topological hypersurfaces would host nearly or absolutely flat, midgap hypersurface bands, depending on whether the number of the hyperlayers is even

or odd, similar to the 3D SSH systems. Computational demonstrations of such flat bands for the ND topological

SSH systems with open hypersurfaces are left for future studies.

[S1] K. Qian, L. Zhu, K. H. Ahn, and C. Prodan, Observation of flat frequency bands at open edges and antiphase

boundary seams in topological mechanical metamaterials, Phys. Rev. Lett. **125**, 225501 (2020).

SSH chains	$\alpha_1, \alpha_2, \dots, \alpha_N$	$\beta_1 \ \beta_2 \ \dots \ \beta_n \ \dots \ \beta_N$	ν_1	$\nu_2 \ \nu_3 \ \dots \ \nu_n \ \dots \ \nu_N$	TI/nonTI
Along \hat{x}_1	$\alpha_1 > \sum_{m \neq 1} \alpha_m$	$\begin{matrix} + & 0 & \dots & 0 & \dots & 0 \\ - & 0 & \dots & 0 & \dots & 0 \end{matrix}$	$\begin{matrix} 0 \\ 1 \end{matrix}$	$\begin{matrix} 0 & 0 & 0 & \dots & 0 & \dots & 0 \\ 0 & 0 & 0 & \dots & 0 & \dots & 0 \end{matrix}$	$\begin{matrix} \text{nonTI} \\ \text{TI} \end{matrix}$
Along \hat{x}_2	$\alpha_2 > \sum_{m \neq 2} \alpha_m$	$\begin{matrix} 0 & + & \dots & 0 & \dots & 0 \\ 0 & - & \dots & 0 & \dots & 0 \end{matrix}$	$\begin{matrix} 0 \\ 1 \end{matrix}$	$\begin{matrix} -1 & 0 & \dots & 0 & \dots & 0 \\ 1 & 0 & \dots & 0 & \dots & 0 \end{matrix}$	$\begin{matrix} \text{TI} \\ \text{TI} \end{matrix}$
\vdots	\vdots	$\vdots \ \vdots \ \vdots \ \vdots \ \vdots \ \vdots$	\vdots	$\vdots \ \vdots \ \vdots \ \vdots \ \vdots \ \vdots$	\vdots
Along \hat{x}_n	$\alpha_n > \sum_{m \neq n} \alpha_m$	$\begin{matrix} 0 & 0 & \dots & + & \dots & 0 \\ 0 & 0 & \dots & - & \dots & 0 \end{matrix}$	$\begin{matrix} 0 \\ 1 \end{matrix}$	$\begin{matrix} 0 & 0 & 0 & \dots & -1 & \dots & 0 \\ 0 & 0 & 0 & \dots & 1 & \dots & 0 \end{matrix}$	$\begin{matrix} \text{TI} \\ \text{TI} \end{matrix}$
\vdots	\vdots	$\vdots \ \vdots \ \vdots \ \vdots \ \vdots \ \vdots$	\vdots	$\vdots \ \vdots \ \vdots \ \vdots \ \vdots \ \vdots$	\vdots
Along \hat{x}_N	$\alpha_N > \sum_{m \neq N} \alpha_m$	$\begin{matrix} 0 & 0 & \dots & 0 & \dots & + \\ 0 & 0 & \dots & 0 & \dots & - \end{matrix}$	$\begin{matrix} 0 \\ 1 \end{matrix}$	$\begin{matrix} 0 & 0 & 0 & \dots & 0 & \dots & -1 \\ 0 & 0 & 0 & \dots & 0 & \dots & 1 \end{matrix}$	$\begin{matrix} \text{TI} \\ \text{TI} \end{matrix}$

TABLE S1. Winding numbers ν_n with $n = 1, 2, \dots, N$ for the hypersurfaces parallel to all \mathbf{a}_m 's with $m \neq n$ for the ND SSH systems. The parameters α_n and β_n with $n = 1, 2, \dots, N$ are the parameters of the ND SSH Hamiltonian in Eq. (S9), associated with the distortions. TI and nonTI mean topological and nontopological insulators, respectively.